

ITER plasma current and shape control using MPC*

Samo Gerkšič and Gianmaria De Tommasi, *Member, IEEE*

Abstract— In plasma magnetic control schemes, comprising a cascade control scheme with a plasma current and shape controller (CSC) in the outer loop and a vertical stabilisation (VS) controller in the inner loop, the main challenges are: the suppression of plasma shape transients after disturbances specific to tokamak reactors; the robustness to changes of the local dynamics; using the available chamber volume in the best possible way, so that the plasma is placed as close as possible to the plasma facing components; and tight control near power supply and gap constraints. Model predictive control (MPC) is an advanced process control approach for dealing with constraints, already established in a range of industries involving multivariable processes with slower dynamics. In this work we present an MPC controller for the ITER CSC in order to assess the feasibility of its practical implementation, and a performance evaluation in comparison to a CSC based on singular perturbation decomposition (SPD).

I. INTRODUCTION

In a magnetically confined fusion reactor, the plasma current and shape controller (CSC) is the component of plasma magnetic control (PMC) that commands the voltages applied to the poloidal field coils, to control the coil currents and the plasma parameters, such as the plasma shape, current, and position. The CSC acts on the system pre-stabilised by the inner vertical stabilisation (VS) controller. The task of PMC is to maintain the prescribed plasma shape and plasma-wall distances (gaps), in presence of disturbances, such as vertical displacement events (VDE), H-L transitions or edge-localised modes (ELM), and to changes of local dynamics in different operating points [1, 2]. In order to achieve high performance, control methods that would improve the performance near the vessel boundaries and the actuator constraints are desired.

Model Predictive Control (MPC) is an established advanced process control approach in the process industry. It has gained wide industrial acceptance by facilitating a systematic approach to control of large-scale multivariable systems, with efficient handling of constraints on process variables and enabling plant optimisation [3]. These advantages are considered beneficial for PCSC, and potentially also for other control systems of a tokamak. The

*Research supported by Slovenian Research Agency (P2-0001). This work has been carried out within the framework of the EUROfusion Consortium and has received funding from the Euratom research and training programme 2014-2018 under grant agreement No 633053. The views and opinions expressed herein do not necessarily reflect those of the European Commission.

Samo Gerkšič is with Jožef Stefan Institute, Jamova 39, Ljubljana, Slovenia (phone: +386 1 477 3665; e-mail: samo.gerksic@ijs.si).

Gianmaria De Tommasi is with Univ. di Napoli Federico II / DIETI / Consorzio CREATE, Via Claudio 21, 80125, Napoli, Italy (e-mail: detommas@unina.it).

main obstacle to using MPC for control of such processes is the restriction of the most relevant MPC methods to processes with relatively slow dynamics due to the long achievable sampling rates, typically needed for the on-line optimisation. However, speeding up MPC has been a topic of intensive research recently [4, 5, 6].

In this work we present an MPC controller for the ITER CSC in order to assess the feasibility of its practical implementation. A performance evaluation in simulation in comparison to a CSC based on singular perturbation decomposition (SPD) [7] is shown, using the VS scheme [8]. The structure of the paper is as follows. In Section 2, the control problem and simulation setup is outlined. Section 3 briefly describes the VS, and Section 4 the proposed MPC CSC. In Section 5, the results are presented and discussed.

II. MAGNETIC PLASMA CONTROL SIMULATION SETUP

The simulations and controller design methods are based on high-order local linear dynamical models of the tokamak plasma from CREATE-L or CREATE-NL [9, 10], at several different equilibrium points, defined by the nominal plasma current I_p , poloidal beta β_p , and internal inductance l_i , for the anticipated ITER plasma. The models are listed in Table I.

TABLE I. LOCAL LINEAR DYNAMIC MODELS.

Model code	I_p (MA)	β_p	l_i	Number of states
LM52	15.0	0.10	0.80	123
LM53	15.0	0.10	1.00	123
LM59	15.0	0.60	0.60	123
LM60	15.0	0.60	0.80	123
LMNE	15.0	0.10	1.21	120

The Matlab/Simulink simulation scheme comprises:

- the plasma/circuits linearized model,
- a simplified model of plasma diagnostics for the plasma vertical velocity v_p and position z_p (a first-order dynamic lag filter with the time constant equal to $7 \cdot 10^{-3}$ s is considered),
- simplified models of the power supplies for the superconductive coils VS1 and for the in-vessel ohmic coils VS3 (a first-order dynamic lag with the time constant equal to $7.5 \cdot 10^{-3}$ s; a delay equal to $2.5 \cdot 10^{-3}$ s; saturations ± 6 kV and ± 1.5 kV for VS1 and VS3, respectively),
- simplified models of the main power supplies (saturations ± 1.5 kV, except for VCS1 ± 3 kV, and first-order dynamic lag with the time constant equal to 0.015 s and a delay equal to 0.015 s),
- the inner cascade control loop of the VS system, which aims at vertically stabilizing the plasma column,

- the outer cascade control loop of the SC, which controls plasma current and shape,
- blocks enabling the simulation of vertical displacement events (VDE), using a corresponding plasma model initial state, and H-L transitions, by injecting recorded profiles of β_p and l_i (BPLI) [11].

The simulation solver ode23tb is used, with relative tolerance 10^{-5} .

III. VERTICAL STABILISATION

For vertical stabilisation, a variant of continuous-time LQG controller which also controls plasma position z_p (ctLQGz) [8] is used.

The ctLQGz VS controller act on the control variables $\mathbf{u}_{VS} = [u_{VS,1} \ u_{VS,2}]^T$, where:

- $u_{VS,1}$ is the voltage applied to the IV coils VS3,
- $u_{VS,2}$ is the voltage applied to the SC circuit VS1,

while it attempts to drive to zero the controlled inputs $\mathbf{y}_{VS} = [y_{VS,1} \ y_{VS,2} \ y_{VS,3}]^T$, where

- $y_{VS,1}$ is the VS3 power supply current,
- $y_{VS,2}$ is the plasma vertical velocity v_p ,
- $y_{VS,3}$ is the plasma vertical position z_p .

It is built by firstly designing a basic ctLQG controller [12, 8] governing only $[y_{VS,1} \ y_{VS,2}]^T$, with a third-order model $\{\mathbf{A}_r, \mathbf{B}_r, \mathbf{C}_r, \mathbf{0}\}$ obtained from a nominal model with model reduction. The LQ controller is tuned by adjusting the diagonal elements of the cost matrices $\mathbf{Q}_{C,y}$ and $\mathbf{R}_{C,u}$, and the covariance matrices of the Kalman filter (KF) are tuned by using $\mathbf{Q}_{K,y} = \mathbf{B}_r \mathbf{B}_r^T$ and tuning the diagonal elements of $\mathbf{R}_{K,y}$ [8]. Then, the additional control loop from z_p is added by augmenting the nominal model with an integrator

$$\mathbf{A}_a = \begin{bmatrix} \mathbf{A}_r & \mathbf{0}_{3 \times 1} \\ \mathbf{C}_{r,2} & 0 \end{bmatrix}, \quad \mathbf{B}_a = \begin{bmatrix} \mathbf{B}_r \\ \mathbf{0}_{2 \times 1} \end{bmatrix}, \quad \mathbf{C}_a = \begin{bmatrix} \mathbf{C}_r & \mathbf{0}_{2 \times 1} \\ \mathbf{0}_{1 \times 3} & 1 \end{bmatrix} \quad (1)$$

where $\mathbf{C}_r^T = [\mathbf{C}_{r,1}^T \ \mathbf{C}_{r,2}^T]$.

IV. PLASMA CURRENT AND SHAPE CONTROLLER

The CSC output is the vector of the 11 main power supply voltages \mathbf{V}_{PF} .

The CSC inputs may include:

- the vector of controlled gaps \mathbf{g} , comprising four gaps and two strike-points,
- the plasma current I_p ,
- the currents in the 11 superconductive coils \mathbf{I}_{PF} .
- the plasma vertical position z_p and the VS3 power supply current I_{VS3} may also be considered, although they are controlled by the VS.

A. Model predictive control (MPC)

The MPC CSC presented in this study is based on the nominal plasma model LM52 in the state-space form. The simplified models of the power supplies and sensors (diagnostics) are appended. Then, the ctLQGz VS feedback loop is added, and the subsystem from the process inputs

$\mathbf{u}_{CSC} = \mathbf{V}_{PF}$ to the outputs $\mathbf{y}_{CSC} = [\mathbf{I}_{PF} \ I_{VS3} \ z_p \ I_p \ \mathbf{g}]^T$ is extracted. With a model reduction procedure, the order of the subsystem is reduced from 199 to 44. The base model for the MCP CSC $\{\mathbf{A}_{CSC}, \mathbf{B}_{CSC}, \mathbf{C}_{CSC}, \mathbf{0}\}$ is finally obtained with model conversion to discrete time with the sampling time $T_s = 0.1$ s, assuming zero-order hold.

For the purposes of this study, the CSC should facilitate offset-free control of I_p and \mathbf{g} to zero with integral action, without set-point tracking. In our implementation, integral action is based on the *disturbance estimation* (DE) concept [13], and the *velocity form* (without tracking) is used to prevent offset due to the control cost when the control signal is non-zero at the steady-state.

For the estimation of asymptotically non-zero disturbances, the base model is augmented with DE integrators at the outputs which require offset-free control. Consider the discrete-time state-space model

$$\begin{aligned} \mathbf{x}(k+1) &= \mathbf{A}\mathbf{x}(k) + \mathbf{B}\mathbf{u}(k) + \mathbf{w}(k), \\ \mathbf{y}(k) &= \mathbf{C}\mathbf{x}(k) + \mathbf{v}(k) \end{aligned} \quad (2)$$

where \mathbf{w} and \mathbf{v} are white noise signals to the state and output, respectively. DE integrator states \mathbf{d} with the associated white-noise signal \mathbf{w}_d are appended to the state \mathbf{x} , so that the augmented state is $\mathbf{x}_a = [\mathbf{x}^T \ \mathbf{d}^T]^T$, and $\mathbf{w}_a = [\mathbf{w}^T \ \mathbf{w}_d^T]^T$. The augmented system is

$$\begin{aligned} \begin{bmatrix} \mathbf{x}(k+1) \\ \mathbf{d}(k+1) \end{bmatrix} &= \begin{bmatrix} \mathbf{A} & \mathbf{0} \\ \mathbf{0} & \mathbf{I} \end{bmatrix} \begin{bmatrix} \mathbf{x}(k) \\ \mathbf{d}(k) \end{bmatrix} + \begin{bmatrix} \mathbf{B} \\ \mathbf{0} \end{bmatrix} u(k) + \begin{bmatrix} \mathbf{I} & \mathbf{0} \\ \mathbf{0} & \mathbf{I} \end{bmatrix} \begin{bmatrix} \mathbf{w}(k) \\ \mathbf{w}_d(k) \end{bmatrix} \\ \mathbf{y}(k) &= [\mathbf{C} \ \mathbf{I}] \begin{bmatrix} \mathbf{x}(k) \\ \mathbf{d}(k) \end{bmatrix} + \mathbf{v}(k) \end{aligned} \quad (3)$$

and is rewritten as

$$\begin{aligned} \mathbf{x}_a(k+1) &= \mathbf{A}_a \mathbf{x}_a(k) + \mathbf{B}_a \mathbf{u}_a(k) + \mathbf{w}_a(k), \\ \mathbf{y}(k) &= \mathbf{C}_a \mathbf{x}_a(k) + \mathbf{v}(k) \end{aligned} \quad (4)$$

The steady-state Kalman filter (KF)

$$\begin{aligned} \mathbf{x}_a(k/k-1) &= \mathbf{A}_a \mathbf{x}_a(k-1/k-1) + \mathbf{B}_a \mathbf{u}(k-1) \\ \mathbf{x}_a(k/k) &= \mathbf{x}_a(k/k-1) + \mathbf{M}_K [\mathbf{y}(k) - \mathbf{C}_a \mathbf{x}_a(k/k-1)] \end{aligned} \quad (5)$$

is used state estimation with the disturbance-augmented model, where \mathbf{M}_K is computed via the steady-state solution of the Riccati equation from the covariance matrices $\mathbf{Q}_K = \mathbf{E}\{\mathbf{w}_a \mathbf{w}_a^T\}$ and $\mathbf{R}_K = \mathbf{E}\{\mathbf{v} \mathbf{v}^T\}$. The KF is used in the sense of an observer, where the diagonal elements of \mathbf{Q}_K and \mathbf{R}_K are used as tuning parameters to achieve desired dynamics.

For the velocity form, the disturbance-augmented system $\{\mathbf{A}_a, \mathbf{B}_a, \mathbf{C}_a, \mathbf{0}\}$ is augmented again. In the velocity-augmentation, the change of the input signal $\delta \mathbf{u}$ becomes the new input; the state expands to $\mathbf{x}_{av} = [\mathbf{x}_a^T \ \mathbf{u}(k-1)^T]^T$; the new output is $\mathbf{y}_{av} = [\mathbf{y}_a^T \ \mathbf{u}(k-1)^T]^T$

$$\begin{aligned} \begin{bmatrix} \mathbf{x}_a(k+1) \\ \mathbf{u}(k) \end{bmatrix} &= \begin{bmatrix} \mathbf{A}_a & \mathbf{B}_a \\ \mathbf{0} & \mathbf{I} \end{bmatrix} \begin{bmatrix} \mathbf{x}_a(k) \\ \mathbf{u}(k-1) \end{bmatrix} + \begin{bmatrix} \mathbf{B}_a \\ \mathbf{0} \end{bmatrix} \delta \mathbf{u}(k) \\ \begin{bmatrix} \mathbf{y}_a(k) \\ \mathbf{u}(k-1) \end{bmatrix} &= \begin{bmatrix} \mathbf{C}_a & \mathbf{D}_a \\ \mathbf{0} & \mathbf{I} \end{bmatrix} \begin{bmatrix} \mathbf{x}_a(k) \\ \mathbf{u}(k-1) \end{bmatrix} + \begin{bmatrix} \mathbf{D}_a \\ \mathbf{0} \end{bmatrix} \delta \mathbf{u}(k) \end{aligned} \quad (6)$$

with $\mathbf{D}_a = \mathbf{0}$ rewritten as

$$\begin{aligned}\mathbf{x}_{av}(k+1) &= \mathbf{A}_{av}\mathbf{x}_{av}(k) + \mathbf{B}_{av}\delta\mathbf{u}(k) \\ \mathbf{y}_{av}(k) &= \mathbf{C}_{av}\mathbf{x}_{av}(k)\end{aligned}\quad (7)$$

Then, the MPC controller is built using the Multi-Parametric Toolbox (MPT) [4] in the output-cost formulation, with the cost function

$$J(\delta\tilde{\mathbf{u}}) = \sum_{k=0}^{N-1} \mathbf{y}_{av,k}^T \begin{bmatrix} \mathbf{Q}_{C,y} & \mathbf{0} \\ \mathbf{0} & \mathbf{0} \end{bmatrix} \mathbf{y}_{av,k} + \delta\tilde{\mathbf{u}}_k^T \mathbf{R}_{C,\delta\tilde{\mathbf{u}}} \delta\tilde{\mathbf{u}}_k \quad (8)$$

where the diagonal elements of the cost matrices for the outputs $\mathbf{Q}_{C,y}$ and the control moves $\mathbf{R}_{C,\delta\tilde{\mathbf{u}}}$ are used as tuning parameters, where $N = 30$ is the prediction horizon length. The control law is obtained by minimising J with respect to the vector of the future control moves $\delta\tilde{\mathbf{u}}$ subject to constraints (currently, only control amplitude constraints $\mathbf{u}_{\min} \leq \mathbf{u} \leq \mathbf{u}_{\max}$ are used). To reduce the computational demand, the number of free control moves is reduced from 30 to 3 using move blocking to intervals [22–26]. Due to the finite horizon length, the control law is computed as a least-squares problem in the unconstrained case, or as a quadratic programming problem in the constrained case [13].

B. Singular perturbation decomposition (SPD)

For comparison, the plasma current and shape control algorithm based on SPD of Ariola and Pironti [7] is used. The SPD CSC implements a multivariable proportional-integral control law from \mathbf{g} and I_p , with an additional proportional contribution from \mathbf{I}_{PF} . It also includes windup protection in case of actuator saturation.

V. SIMULATION RESULTS

Table II lists RISE values (root integral squared error, from the corresponding equilibrium point) of the main process signals in 25 s simulations using the same ctLQGz VS controller,

- with either the MPC or the SPD CSC,
- for VDE events with the initial amplitude -0.1 m and for BPLI disturbances,
- with the five local models, to roughly assess the sensitivity to the varying operating conditions.

Figs. 1-2 show the main process signals in VDE events, and Figs. 3-7 with BPLI disturbances, respectively, simulated in the same time interval; only the simulations with the models LM53 and LM52 are included; the performance with MPC is compared with SPD. "Delta" signal values (the deviations from the equilibrium point of the linear model) are displayed.

The results of the MPC and the SPD scheme are difficult to compare because both methods involve a large number of degrees of freedom in tuning that allow various trade-offs, and the presented simulation results only show the performance with particular sets of tuning parameters. With MPC we have achieved a generally faster suppression of disturbances at I_p and better at \mathbf{g} . The z_p response is mostly improved in BPLI simulations but is slower in VDE simulations. The improved tracking performance comes at the price of a slight increase of the voltages \mathbf{V}_{PF} and

currents \mathbf{I}_{PF} , but there are no rapid reactions indicating oversensitivity.

Fig. 7 shows a simulation similar to the one in Fig. 5, where, in addition to \mathbf{u} constraints, soft constraints $\max(\mathbf{I}_{PF}) \leq 4$ kA were set in the MPC controller. It is not feasible to fully adhere to this limit, yet the controller manages to reduce the current peaks visibly.

VI. CONCLUSION

The study has so far shown that efficient simulation performance in plasma CSC is achievable using MPC and that limitation of coil currents is possible without using an additional intermediate cascade loop for \mathbf{I}_{PF} control. Traditionally, MPC was not considered applicable to control problems of such scale with sub-second sampling intervals; however, preliminary research results outside the scope of this paper indicate that computation times of 10 ms are achievable using fast online optimization methods combined with complexity-reduction approaches. We also intend to pursue improvements of performance near constraints, and tools for tuning support using local linear analysis.

ACKNOWLEDGMENT

We gratefully acknowledge the collaboration of CosyLab, d.d..

REFERENCES

- [1] T. Bellizio et al., "Control of elongated plasma in presence of ELMs in the JET tokamak," *IEEE T. Nucl. Sci.*, vol. 58, Aug. 2011, pp. 1497–1502.
- [2] A. Neto et al., "Exploitation of Modularity in the JET Tokamak VS System," *Control Eng. Pract.*, vol. 20, no. 9, 2012, pp. 846–856.
- [3] S. J. Qin and T. A. Badgwell, "A survey of industrial model predictive control technology," *Control Eng. Pract.*, vol. 11, 2003, pp. 733–764.
- [4] Kvasnica, M.: *Real-time model predictive control via multi-parametric programming*. Saarbrücken: VDM verlag, 2009.
- [5] M. N. Zeilinger, C. Jones, and M. Morari, "Real-time suboptimal Model Predictive Control using a combination of Explicit MPC and Online Optimization," *IEEE Trans. Auto. Contr.*, vol. 56, 2011, pp. 1524–1534.
- [6] E. N. Hartley et al., "Predictive control using an FPGA with application to aircraft control," *IEEE Trans. Control Systems Technology*, vol. 22, 2014, pp. 1006–1017.
- [7] M. Ariola and A. Pironti, "An Application of the Singular Perturbation Decomposition to Plasma Position and Shape Control," *Eur. J. Control*, vol. 9, 2003, pp. 410–420.
- [8] S. Gerškšič, G. De Tommasi, "Improving magnetic plasma control for ITER," *Fusion Eng. Des.*, vol. 89, 2014, pp. 2477–2488.
- [9] R. Albanese and F. Villone, "The linearized CREATE-L plasma response model for the control of current, position and shape in tokamaks," *Nucl. Fus.*, vol. 38, 1998, pp. 723–738.
- [10] R. Albanese, G. Calabro, M. Mattei, and F. Villone, "Plasma response models for current, shape and position control at JET," *Fusion Eng. Des.*, vol. 66–68, 2003, pp. 715–718.
- [11] G. Ambrosino, M. Ariola, G. De Tommasi, A. Pironti, and A. Portone, "Design of the Plasma Position and Shape Control in the ITER Tokamak Using In-Vessel Coils," *IEEE Trans. Plasma Science*, vol. 37, 2009, pp. 1324–1331.
- [12] S. Gerškšič and G. De Tommasi, "Vertical stabilization of ITER plasma using explicit model predictive control," *Fusion Eng. Des.*, vol. 88, 2013, pp. 1082–1086.
- [13] S. Gerškšič and B. Pregelj, "Tuning of a tracking multi-parametric predictive controller using local linear analysis," *IET Control Theory Appl.*, vol. 6, 2012, pp. 1–11.

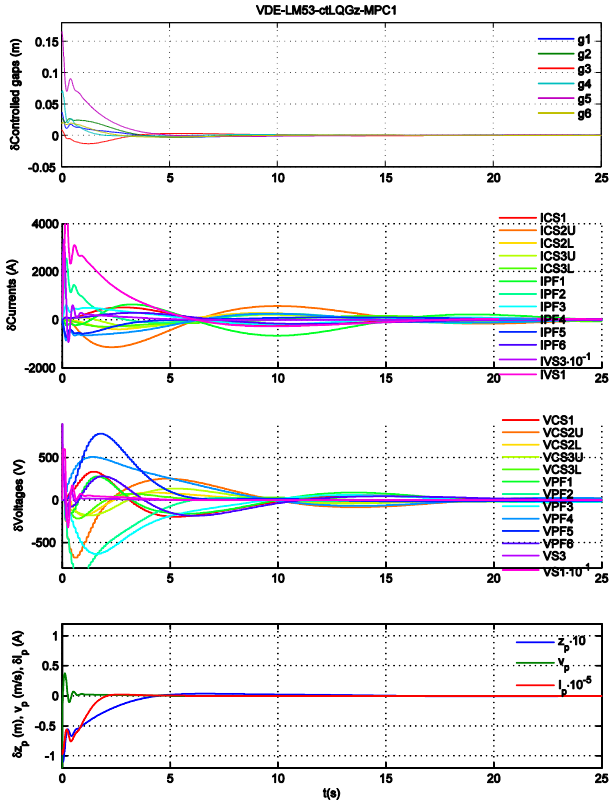


Fig. 1. VDE simulation: ctLQGz-MPC, model LM53.

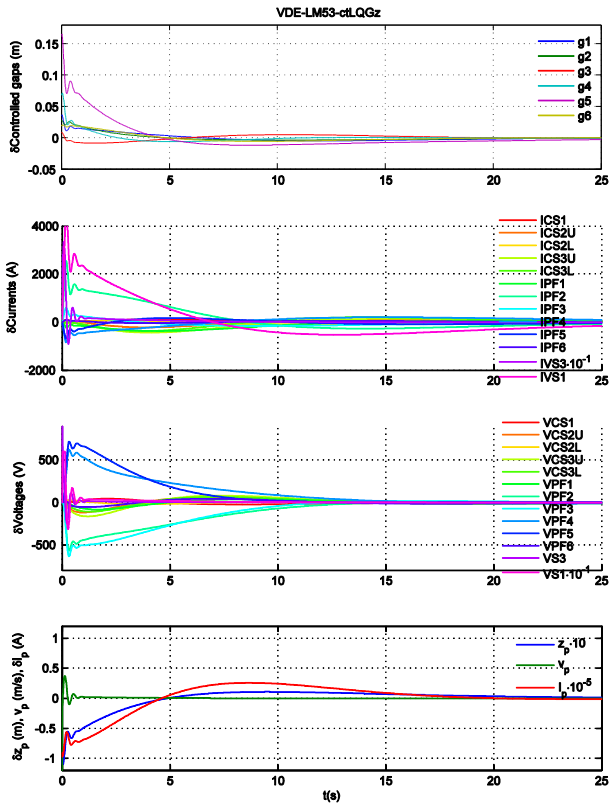


Fig. 2. VDE simulation: ctLQGz-SPD, model LM53.

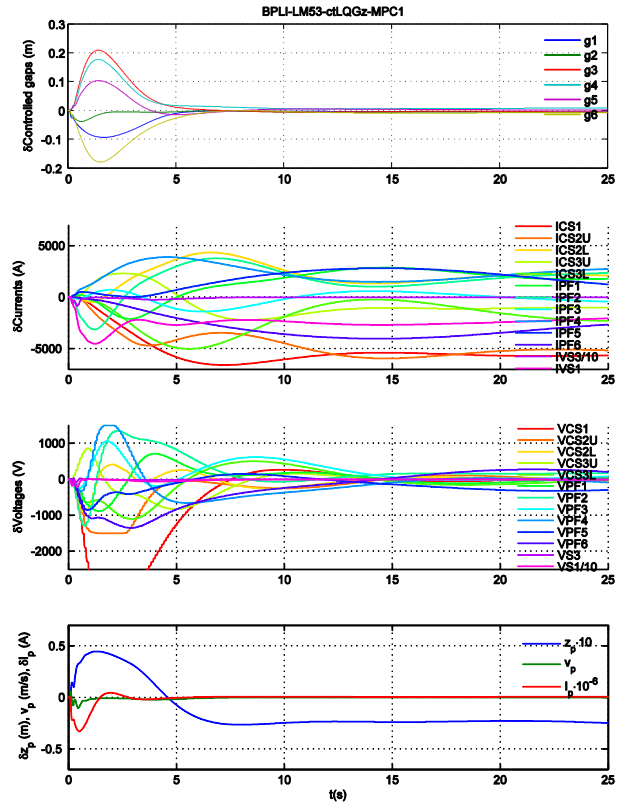


Fig. 3. BPLI simulation: ctLQGz-MPC, model LM53.

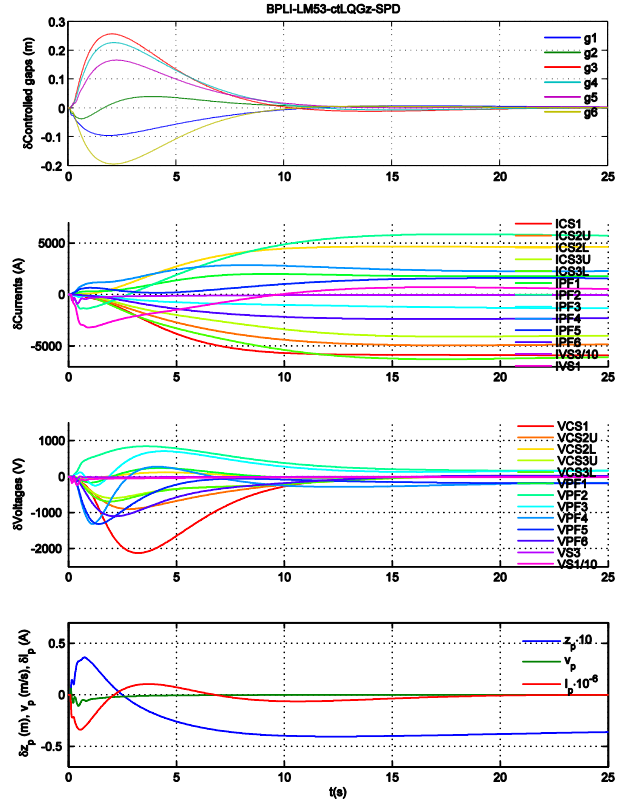


Fig. 4. BPLI simulation: ctLQGz-SPD, model LM53.

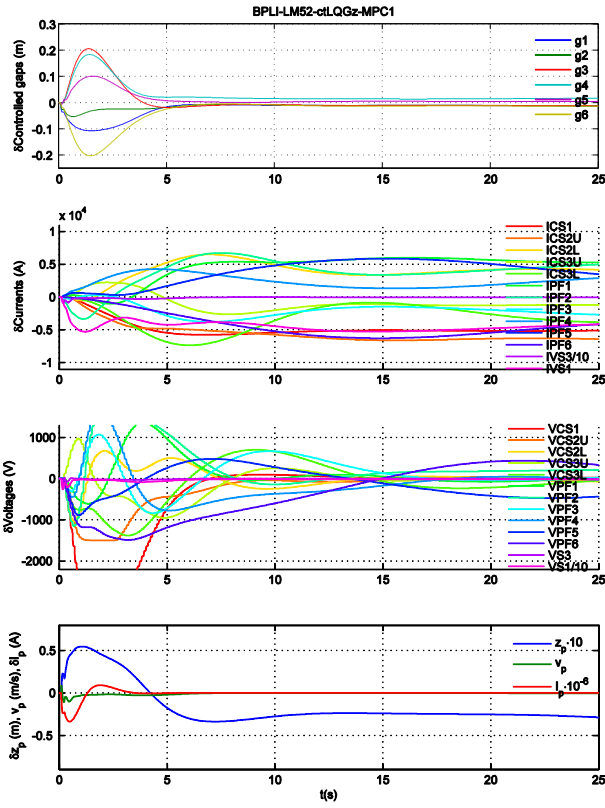


Fig. 5. BPLI simulation: ctLQGz-MPC, model LM52.

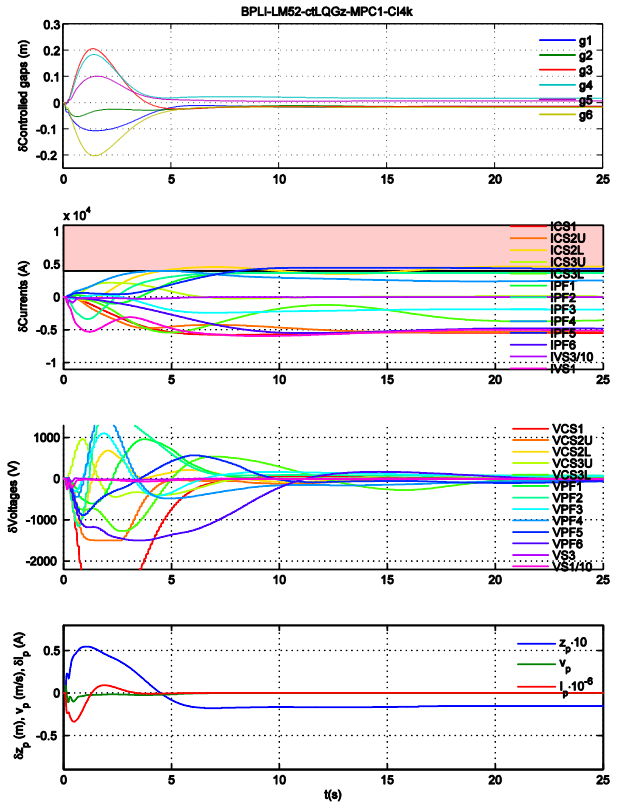


Fig. 7. BPLI simulation: ctLQGz-MPC, model LM52, with soft constraints $\max(I_{PF}) \leq 4$ kA.

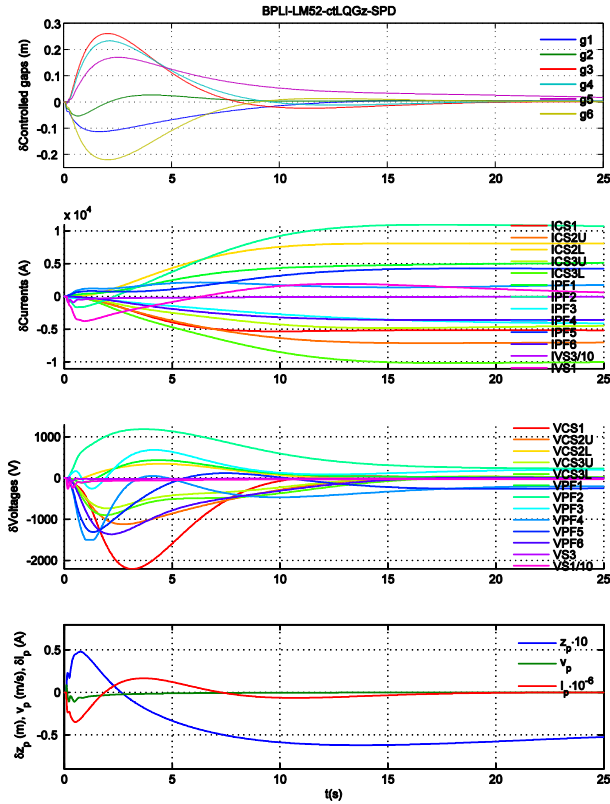


Fig. 6. BPLI simulation: ctLQGz-SPD, model LM52.

TABLE II. RISE VALUES (FROM THE CORRESPONDING EQUILIBRIUM).

LMNE	VDE-ctLQGz-MPC	VDE-ctLQGz-SPD	BPLI-ctLQGz-MPC	BPLI-ctLQGz-SPD
max(CtrlGaps)	0.067183	0.07322	0.24188	0.6735
avg(CtrlGaps)	0.019551	0.02092	0.16442	0.447
max(AllGaps)	0.088145	0.09702	0.48326	1.0339
avg(AllGaps)	0.017834	0.01875	0.20083	0.48994
IVS3	36320	36357	7358.9	8557.4
IVS1	1262	1344.2	4731.5	7366.8
VS3	97.011	97.126	17.127	65.23
VS1	3264.5	3283.2	1420.5	2411.2
v_p	0.6012	0.60184	0.11636	0.087254
z_p	0.025029	0.02783	0.087254	0.25402
I_p	25926	31177	442220	575550
LM52	VDE-ctLQGz-MPC	VDE-ctLQGz-SPD	BPLI-ctLQGz-MPC	BPLI-ctLQGz-SPD
max(CtrlGaps)	0.11312	0.13224	0.28927	0.45392
avg(CtrlGaps)	0.03931	0.04727	0.19914	0.32625
max(AllGaps)	0.21748	0.24904	0.6673	1.2303
avg(AllGaps)	0.052378	0.06047	0.2547	0.42863
IVS3	10014	9840.8	6860.6	8539.7
IVS1	3861	4097.4	22622	8149.3
VS3	158.11	156.92	63.439	69.548
VS1	2484.3	2435.7	1825.7	2412.4
v_p	0.13284	0.13179	0.075632	0.086616
z_p	0.082884	0.09539	0.14286	0.26018
I_p	79948	134900	275000	431300
LM53	VDE-ctLQGz-MPC	VDE-ctLQGz-SPD	BPLI-ctLQGz-MPC	BPLI-ctLQGz-SPD
max(CtrlGaps)	0.10138	0.11235	0.27591	0.46948
avg(CtrlGaps)	0.037829	0.04289	0.18146	0.30869
max(AllGaps)	0.25307	0.28416	0.56506	0.8483
avg(AllGaps)	0.055365	0.06094	0.2296	0.36091
IVS3	11949	11860	5730.9	6909.6
IVS1	4075.3	4311.1	12920	5927
VS3	192.85	192.27	54.533	56.088
VS1	2615.1	2586.5	1548.7	1897.1
v_p	0.16552	0.16504	0.062971	0.073573
z_p	0.078885	0.08749	0.12626	0.17578
I_p	68748	122600	265130	380330
LM59	VDE-ctLQGz-MPC	VDE-ctLQGz-SPD	BPLI-ctLQGz-MPC	BPLI-ctLQGz-SPD
max(CtrlGaps)	0.12084	0.16562	0.30581	0.54037
avg(CtrlGaps)	0.048016	0.05993	0.25257	0.29891
max(AllGaps)	0.20879	0.28263	1.2666	2.3938
avg(AllGaps)	0.059293	0.07147	0.41902	0.58263
IVS3	9016.3	8624.3	8502.6	10344
IVS1	3401.4	3459	55016	7778.7
VS3	134.88	132.64	86.887	94.695
VS1	2623.4	2533.1	2282.3	3016.1
v_p	0.10447	0.10228	0.091223	0.10034
z_p	0.091871	0.11635	0.15196	0.35798
I_p	128420	192320	291360	378100
LM60	VDE-ctLQGz-MPC	VDE-ctLQGz-SPD	BPLI-ctLQGz-MPC	BPLI-ctLQGz-SPD
max(CtrlGaps)	0.14021	0.17821	0.36421	0.6735
avg(CtrlGaps)	0.049426	0.06082	0.23439	0.447
max(AllGaps)	0.25214	0.29641	0.68351	1.0339
avg(AllGaps)	0.062564	0.07296	0.28841	0.48994
IVS3	8424.5	7989.6	6378.5	8557.4
IVS1	3923.5	4168.2	19028	7366.8
VS3	119.07	116.17	55.333	65.23
VS1	2356.3	2248.4	1691.6	2411.2
v_p	0.10323	0.10036	0.071016	0.087254
z_p	0.085086	0.10566	0.13991	0.25402
I_p	79535	120170	308480	575550